Optical waveguide and cavity effects on whispering-gallery mode resonances in a ZnO nanonail

Jinzhang Liu,[1] Quang Minh Ngo,[2] Kyung Ho Park,[3] Sangin Kim,[2] Yeong Hwan Ahn,[1] Ji-Yong Park,[1] Ken Ha Koh,[1] and Soonil Lee[1,a)]

[1]*Division of Energy Systems Research, Ajou University, Suwon 443-749, Republic of Korea*
[2]*Division of Electrical and Computer Engineering, Ajou University, Suwon 443-749, Republic of Korea*
[3]*Korea Advanced Nano Fab Center, Suwon 443-766, Republic of Korea*

Spatially resolved cathodoluminescence (CL) study of a ZnO nanonail, having thin shank, tapered neck, and hexagonal head sections, is reported. Monochromatic imaging and line-scan profiling indicate that the wave guiding and leaking from growth imperfections in addition to the oxygen-deficiency variation determine the spatial contrast of CL emissions. Occurrence of resonance peaks at identical wavelengths regardless of CL-excitation spots is inconsistent with the whispering-gallery mode (WGM) resonances of a two-dimensional cavity in the finite-difference time domain simulation. However, three-dimensioanl cavity simulation produced WGM peaks that are consistent with the experimental spectra, including transverse-electric resonances that are comparable to transverse-magnetic ones. © 2009 American Institute of Physics.
[doi:10.1063/1.3268806]

Crystalline structures that are regularly shaped in submicrometer scale and strongly confine light are attractive for fundamental researches and potential applications in photonics. The studies on waveguiding,[1] resonances,[2] and lasing[3] in submicron crystals are such examples. In recent years, one-dimensional (1D) wurtzite-structure ZnO nanocrystals, in particular, have emerged as attractive photonics material because of their hexagonal cross-section which allows whispering gallery mode (WGM) resonance that is useful for lasing,[4] sensing,[5] and optical modulating.[6]

One of the difficult issues related to the WGM resonance in ZnO 1D structures, such as rod- or needle-shaped crystals in submicrometer scale, is the mode identification because there can be two sets of resonance peaks due to the birefringence of ZnO; the direct polarization-dependent measurement of the photoluminescence (PL) from an individual ZnO nanostructure is difficult. When conventional PL measurements are made from a heap of ZnO nanorods, the size distribution of ZnO nanorods blurs the distinction of individual WGM peaks so that only the WGM peaks with low apparent quality factors are observed. On the contrary, when cathodoluminescence (CL) is used to study the WGM resonance in an individual ZnO nanostructure, a series of prominent peaks appear. However, typically, polarization-dependent CL measurements cannot be made because of the instrumental limitation.

Previously, the preferential occurrence of transverse magnetic (TM)-polarized ($E \parallel c$) modes in the PL spectra of an individual rod- and needle-shaped ZnO microcrystals was reported.[7–9] Moreover, it was claimed that the mode simulations assuming the ZnO microcrystals as two-dimensional (2D) hexagonal (or cylindrical) cavities confirm the unbalanced appearance of transverse electric (TE)- and TM-polarized WGM resonances, with the rare detection of TE modes ($E \perp c$). However, our CL measurements from the

hexagonal head of a single nail-shaped ZnO nanocrystal clearly showed distinct peaks that can be assigned to both TE- and TM-polarized WGM resonances according to the mode equations based on the plane wave (PW) model.[10] On the other hand, a similar phenomena, suppression of TE-polarized resonance, was reported in the study of WGM from a rod-shaped microcrystal of In_2O_3 that has no birefringence.[11] These facts indicate that the suppression of TE-polarized WGM resonance is a characteristic of the 1D microstructures that can be modeled as 2D cavities, regardless of the optical birefringence, and that the nail-shaped nanostructures show very different polarization-dependent WGM resonances because of the additional confinement in the axial direction, which makes it inappropriate to model them as 2D cavities.

In this letter, we investigated the unique CL characteristics of a ZnO nanonail. In addition to the monochromatic CL imaging at the respective wavelengths of 388 and 500 nm, spatially resolved CL spectra were measured along the length of an isolated ZnO nanonail. To elucidate the effect of the additional axial confinement and to identify WGM resonances, we carried out mode simulations based on a more realistic three-dimensional (3D) cavity structure. Our computer simulation is based on the finite-difference time domain (FDTD) method with the perfectly matched layer (PML) boundary conditions.[12]

ZnO nanonails were grown on a silicon substrate through the carbothermal reduction method, the details of which we reported previously.[10] As-grown ZnO nanonails were perpendicular to the substrate, but some nanonails, detached from the substrate during sample cutting, lay parallel to the substrate. A field-emission scanning electron microscope (FE-SEM) (Hitachi S-4300SE) and a CL setup (Gatan MonoCL3+) attached to it were used to characterize ZnO nanonails. All the CL spectra were measured at room temperature by using the electron-beam acceleration voltage of 7 kV.

a)Author to whom correspondence should be addressed. Electronic mail:soonil@ajou.ac.kr.
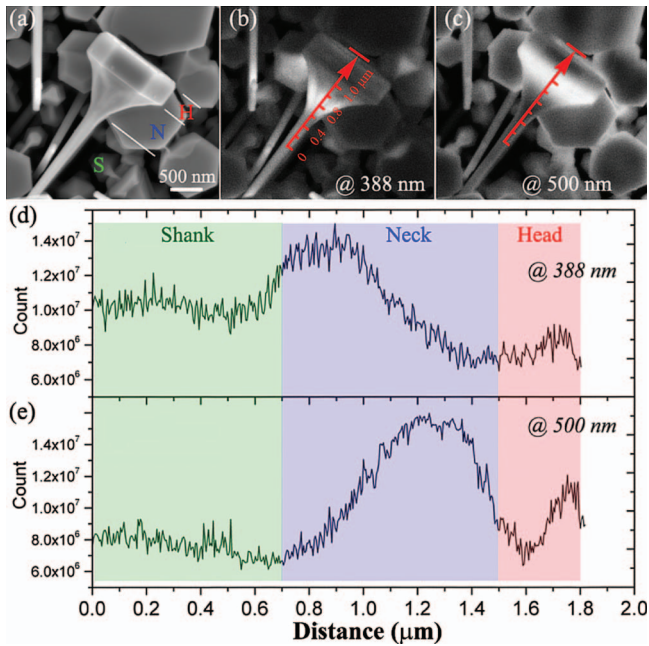
95, 221105-1

FIG. 1. (Color) (a) FE-SEM image of a ZnO nanonail, of which the monochromatic CL images taken at 388 (b) and 500 nm (c) are shown. (d) and (e) Line profiles corresponding to the arrows show CL intensity variations of UV and green emissions, respectively.
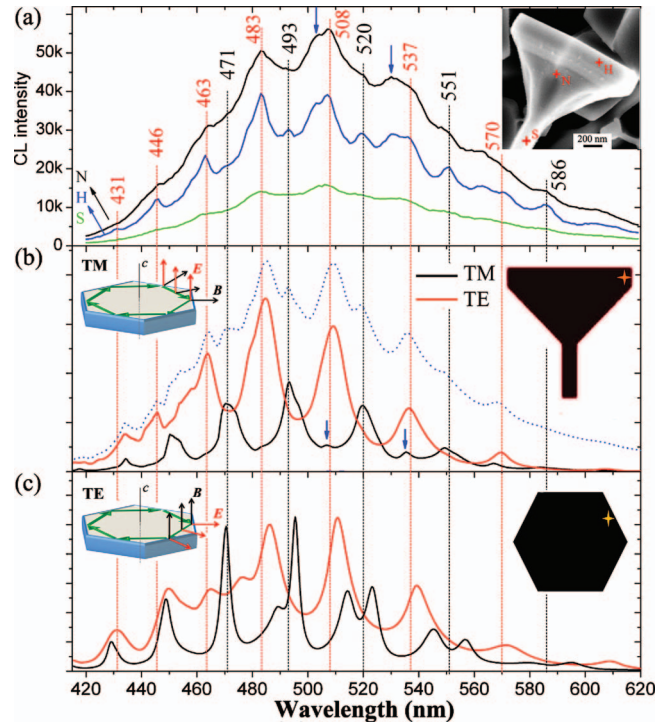

FIG. 2. (Color) (a) CL spectra from a single ZnO nanonail shows a series of resonance peaks at the same wavelengths regardless of the origin of CL. (b) and (c) Simulated TM- and TE-polarized WGMs within a nail-like 3D cavity and a hexagonal 2D cavity, respectively. The cavity radius of 810 nm is used for simulation. The insets on the left-hand side illustrate the configuration of electric and magnetic fields corresponding to TM and TE modes, respectively. The asterisks in the insets on the right-hand side mark the light source positions.

Figure 1(a) shows a FE-SEM image of a ZnO nanonail that consists of a thin shank, a tapered neck section, and a hexagonal head with six well-faceted sides. Figures 1(b) and 1(c) are corresponding monochromatic CL images of the ZnO nanonail taken at the wavelengths of 388 and 500 nm, which are the near band-edge (NBE) and defect-related emission, respectively. We note that the two monochromatic CL images show very different spatial contrast. NBE emission was brightest at the lower part of the tapered neck section [Figs. 1(b) and 1(d)], whereas very intense green emission appeared around the bottom of the hexagonal head where tapered neck joins the head [Figs. 1(c) and 1(e)]. Green emission is known to originate from oxygen deficiency,[13] and, therefore, the bright local green emission indicates that there are large amount of oxygen vacancies at the upper end of the tapered neck. Presumably, there is a correlation between the concentration of oxygen vacancy and the change in growth direction. It appears that initially stoichiometric ZnO rod grows along the *c* axis to become a thin shank, but the lateral growth starts to compete with the axial growth as Zn supply exceeds that of oxygen to result in a tapered neck section. Eventually the *c*-axis growth of ZnO with a slight oxygen deficiency resumes and a large hexagonal head forms. We attribute the low 388 nm emission along the shank to the wave-guiding effect; most of the NBE emission is guided inside the thin shank. However, some portion of the NBE emission leaks from growth imperfections in the tapered neck section.[1]

Figure 2(a) shows spatially resolved visible CL spectra of a ZnO nanonail, the FE-SEM image of which is shown in the inset. The spectra H, N, and S are excited by bombarding the corresponding cross-marked positions in the inset with a 7 keV electron beam under identical conditions. The three positions H, N, and S are at the center of a side facet of the top cap, at the upper section of the tapered neck near a corner, and at the shank, respectively. Spectrum N has the larg-

est intensity that is consistent with the CL image in Fig. 1(c) and the line profile in Fig. 1(e). However, the spectrum H shows the WGM resonances most prominently, which indicates that the hexagonal head functions as a good cavity in spite of the fact that less intense visible CL occurs because of low oxygen vacancies. Interestingly, the positions of the resonance peaks are identical for both the spectra N and H regardless of their apparent quality factor difference. The intensity of the spectrum S is the weakest, in accordance with the CL image in Fig. 1(c) and the line profile in Fig. 1(e). In addition to the lowest oxygen deficiency, the smaller effective generation volume for CL can be responsible for the weakest spectrum; the penetration depth of electrons at the acceleration voltage of 7 kV, which is deduced as ∼350 nm from a Monte Carlo simulation, exceeds the size of the shank. However, the spectrum S shows broad, but clearly discernible, resonance peaks at the wavelengths identical to those in the spectra H and N. Because the WGM wavelengths depend on the size of a resonance cavity, a systematic shift in the resonance peak positions of the three spectra would appear, if the WGM resonances occurred locally at the respective electron bombardment positions.

Within the PW model, the coincidence of resonance-peak positions of the three CL spectra in Fig. 2(a) indicate that the light originating from either the shank or the tapered neck is wave-guided and coupled to the hexagonal head that is the optical cavity responsible for the WGM resonances. However, the classical PW model is not appropriate to elucidate the resonance modes of the submicrometer size cavity. Therefore, we carried out the FDTD-PML simulations to

identify the polarization-dependent WGM resonances and the corresponding radiating-field patterns. Figures 2(b) and 2(c) show the simulation results that are produced by placing either a TM- or TE-polarized Gaussian light pulse at the marked positions inside the 2D and 3D cavities (see the respective insets at right hand). The radii of the 2D cavity and the hexagonal head of the 3D cavity were set at ~810 nm, and the diameter of the shank at ~200 nm, in accordance with the SEM image in the inset of Fig. 2(a). The birefringence of ZnO is taken into account in simulating TE- and TM-polarized resonances by using the $n_e(\lambda)$ and $n_o(\lambda)$ of the epitaxial ZnO film on sapphire.[14]

As shown in Fig. 2(b), 3D-cavity simulation produces good matches of WGM resonance wavelengths with the experimental CL spectra. Moreover, the TE- and TM-polarized WGM resonances are comparable in quality as exhibited by the similar peak widths, and two small TM-peaks denoted by arrows appear as two respective shoulders at 503 and 531 nm. The superposition of the properly weighted TM- and TE-polarization simulations, together with a broad Gaussian luminescence background, reproduced the general features of the experimental spectrum H; see the dotted curve in Fig. 2(b). However, there is a qualitative disagreement between the simulated and experimental spectra in Fig. 2(c). Many of the simulated resonance peaks are redshifted by a few nanometers, the TM-polarized resonances are sharper and more distinct compared to the TE-polarized resonances, and some of the TM-polarized resonances appear in pairs.

We note that the scarce observation of TE-polarized WGM resonances from the rod-type microcrystals[8–11] can be attributed to their 2D-cavity nature. However, it is inappropriate to model the ZnO nanonail as a 2D cavity because the top surface of the hexagonal head provides an additional light confinement in the vertical direction. Therefore, a 3D cavity that mimics the ZnO nanonail is used to simulate polarization-dependent WGM resonances. It seems that the axial confinement of light, which breaks the symmetry of ideal cylinders results in more comparable TM- and TE-polarization WGM resonances. The simulated patterns of radiating fields for some modes in Fig. 3 show that these modes can be easily excited by the electron-beam bombardment at the marked position in Fig. 2(b). The red and blue domains, which switch their positions periodically, denote the positive and negative maxima of field amplitude, respectively. Moreover, these patterns of radiating fields clearly show that the axial losses through the top facet are low, and the lights mainly leak from the upper neck section and the side faces of the top head, in good accordance with the CL image in Fig. 1(c).

In summary, we showed that the waveguiding and 3D cavity effects are important to account for the characteristics of the spatially resolved CL measurements from an individual ZnO nanonail. The spatial CL contrast in the monochromatic imaging and line-scan profiling was attributed to the waveguiding and leaking at the growth imperfections, and the variation in oxygen deficiency. Moreover, the occurrence of WGM resonances at identical wavelengths regardless of the electron excitation positions and apparent quality factor indicated that only the top head functions as a resonance cavity, to which the light generated at other positions have to be guided and coupled. Our FDTD analysis that is more appropriate to elucidate the resonance modes of the
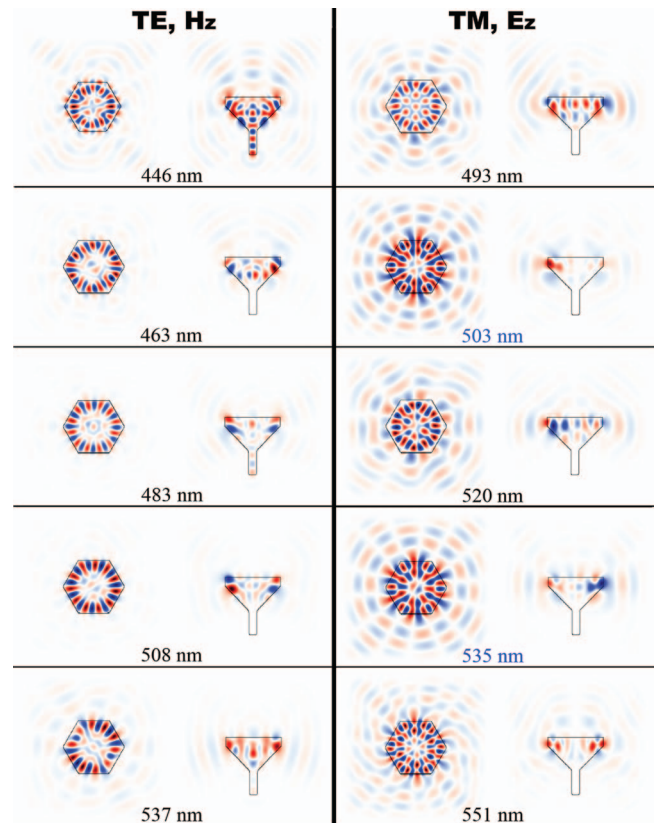

FIG. 3. (Color) Field patterns for the observed modes in Fig. 2(a), corresponding to the light source in head.

submicrometer size cavity showed that modeling the nanonail as a 2D cavity is inadequate. However, FDTD simulation based on a 3D cavity model succeeded in reproducing the general features of the experimental spectrum.

[1] T. Voss, G. T. Svacha, E. Mazur, S. Müller, C. Ronning, D. Konjhodzic, and F. Marlow, Nano Lett. **7**, 3675 (2007).
[2] H. X. Jiang, J. Y. Lin, K. C. Zeng, and W. Yang, Appl. Phys. Lett. **75**, 763 (1999).
[3] M. H. Huang, S. Mao, H. Feick, H. Yan, Y. Wu, H. Kind, E. Weber, R. Russo, and P. Yang, Science **292**, 1897 (2001).
[4] C. Czekalla, C. Sturm, R. Schmidt-Grund, B. Cao, M. Lorenz, and M. Grundmann, Appl. Phys. Lett. **92**, 241102 (2008).
[5] J. Lutti, W. Langbein, and P. Borri, Appl. Phys. Lett. **93**, 151103 (2008).
[6] V. S. Ilchenko, A. B. Matsko, A. A. Savchenkov, and L. Maleki, Proc. SPIE **4629**, 158 (2002).
[7] T. Nobis, E. M. Kaidashev, A. Rahm, M. Lorenz, and M. Grundmann, Phys. Rev. Lett. **93**, 103903 (2004).
[8] N. H. Nickel and E. Terukor, *Zinc Oxide—A Material for Micro- and Optoelectronic Applications* (Springer, The Netherlands, 2005).
[9] T. Nobis and M. Grundmann, Phys. Rev. A **72**, 063806 (2005).
[10] J. Liu, S. Lee, Y. H. Ahn, J.-Y. Park, K. H. Koh, and K. H. Park, Appl. Phys. Lett. **92**, 263102 (2008).
[11] H. Dong, Z. Chen, L. Sun, J. Lu, W. Xie, H. H. Tan, C. Jagadish, and X. Shen, Appl. Phys. Lett. **94**, 173115 (2009).
[12] J.-P. Bérenger, J. Comput. Phys. **127**, 363 (1996).
[13] K. Vanheusden, W. L. Warren, C. H. Seager, D. R. Tallant, J. A. Voigt, and B. E. Gnade, J. Appl. Phys. **79**, 7983 (1996).
[14] C. W. Teng, J. F. Muth, Ü. Özgür, M. J. Bergmann, H. O. Everitt, A. K. Sharma, C. Jin, and J. Narayan, Appl. Phys. Lett. **76**, 979 (2000).